RSC Advances

PAPER

View Article Online
View Journal | View Issue

Cite this: *RSC Adv.*, 2022, **12**, 8737

Dynamic covalent hydrogel of natural product baicalin with antibacterial activities†

Zhen-Zhen Wang, *[a] Yuan Jia,[a] Guoqiang Wang,[a] Hongjuan He,[a] Lihua Cao,[a] Yanmei Shi,[a] Mingsan Miao*[a] and Xiu-Min Li*[bc]

Received 12th October 2021
Accepted 17th February 2022

DOI: 10.1039/d1ra07553e

rsc.li/rsc-advances

Baicalin has been demonstrated to have multiple pharmacological activities but low solubility. Various baicalin hydrogels have been used to improve its solubility and break its limitation in clinical applications. However, traditional baicalin hydrogels contain numerous ingredients and usually show low baicalin loading capacity. Herein, we discovered a dynamic covalent hydrogel only consisting of baicalin and inorganic borate, in which baicalin is considered as the carrier and drug without other ingredients. The dynamic boronate bonds endow the hydrogel with excellent degradability and multi-stimuli-responsiveness. Moreover, the hydrogel displayed remarkable thixotropy, moldability, and self-healing properties. And the biocompatible baicalin hydrogel exhibited significant antibacterial activities, and can be considered as a potential drug delivery system for biomedical applications.

Introduction

Stimuli-responsive hydrogels are intriguing "smart"/functional materials responding to various stimuli such as pH, temperature, ions, redox-regent, enzymes, and UV, and display potential applications in artificial muscles, sensing matrices, 3D-scaffolds of drug delivery, cell culture, and tissue generation.[1–3] Hydrogels are constructed by the linkage of gelators through covalent or non-covalent bonds, forming diverse spatial structures including nanofibers, nanotubes, nanocapsules, films, and foams.[4,5] Generally, the stimuli-responsive properties of hydrogels rely on the special structure design, primarily using polymers with stimuli-responsive covalent bonds[6,7] such as disulfide bonds, thiol-Michael exchange, boronate ester, silyl ether, imine, hemiacetal, and azo, or non-covalent interactions such as host–guest pair recognition.[8,9] Polymer materials are intriguing in drug delivery systems.[10–12] However, tedious design of the structure usually requires tiring synthetic procedures and difficult purifications. Then the hydrogels constructed by small molecules[13,14] emerge through non-covalent bonds such as hydrogen bonds, van der Waals force, and hydrophobic interactions, and display excellent thixotropy, biodegradability, and self-healing behavior.[15–17] However, compared with dynamic covalent chemistry, the stability of such supramolecular hydrogels is still a challenge due to relatively weak intermolecular interactions.[18] Thus, introducing reversible covalent bonds into the small-molecule gelators might be a wise strategy to improve the stability of small-molecule hydrogels.[19]

Traditional Chinese herbs are abundant sources for small-molecule gelators due to the various structural backbone, plentiful functional groups, and special chiral properties.[20] Moreover, the natural small products are excellent biocompatible and biodegradable materials with extensive pharmacological activities. For example, natural small molecules including puerarin,[21] rhein,[22] betulonic acid,[23] berberine,[24] glycyrrhizic acid,[25,26] tricyclic diterpene acids,[27] and triterpenoids[28] were reported to self-assemble into the hydrogel and have displayed various biological activities. To improve the stability and strength of hydrogel formed by natural small products, the application of dynamic covalent linkage in hydrogel still needs to be explored.

The boronate ester, a type of reversible functional groups, is formed between boric acid and catechol, *cis*-1, 2-diol, *cis*-1,3-diol, or α-hydroxy-carboxylic acid.[29–31] The binding affinity is determined by p*K*a of substrate boric acid, the pH value of the environment and the dihedral angle of the substrate diols.[32,33] The dynamic boronate ester has been widely applied in polymeric materials, where boronate ester crosslinking endow the system with fast self-healing ability and enhance the mechanical property.[34–36] However, the direct crosslink of small molecules by boronate ester is barely reported. Recently, the stimuli-responsive hydrogel formed by polyphenol tannic acid with inorganic borate or organic borate has been discovered,[37] which displayed excellent anti-bacterial activities.

Here we discovered a hydrogel formed by natural small product baicalin (BA) cross-linked by boronate ester, which can

[a]*Academy of Chinese Medical Science, Henan University of Chinese Medicine, Zhengzhou, China. E-mail: zzwang@hactcm.edu.cn*

[b]*Department of Pathology, Microbiology & Immunology, New York Medical College, Valhalla, NY, USA. E-mail: XiuMin_Li@NYMC.edu*

[c]*Department of Otolaryngology, New York Medical College, Ardsley, NY, USA*

† Electronic supplementary information (ESI) available. See DOI: 10.1039/d1ra07553e

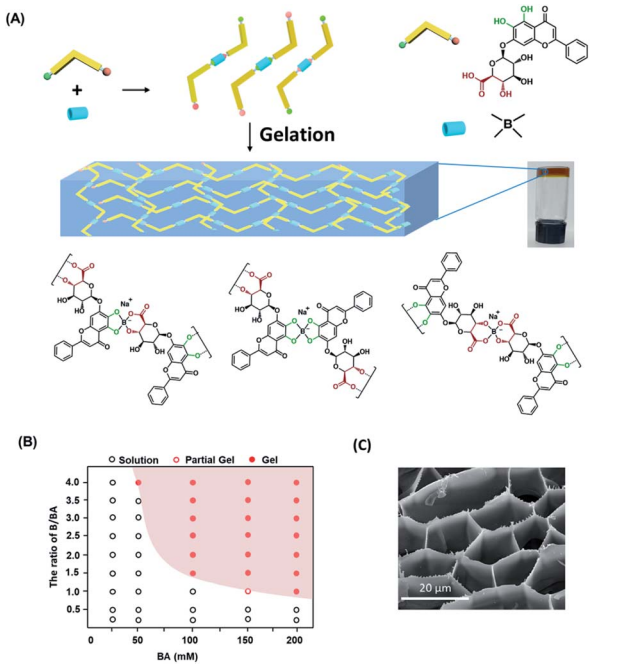

Fig. 1 BA hydrogel. (A) Illustration of BA hydrogels formation; (B) phase diagram of BA–$Na_2B_4O_7$ mixture (the BA, NaOH and inorganic borate salt in deionized water were mixed, heated, and cooled down to observe the sample state). (C) SEM photograph of BA hydrogel (BA : B = 100 mM : 200 mM).

respond to various triggers such as pH and temperature. BA, the major component in herb *Scutellaria baicalensis*, has shown extensive pharmacological activities such as anti-oxidation, anti-inflammation, anti-allergy, and anti-tumor by regulating diverse pathways including $NLRP_3$/caspase-1, TLR4/NF-κB, PI3K/AKT, and AGE/RAGE.[38,39] BA is composed of glucuronic acid as a hydrophilic group with potential hydrogen interactions and flavonoid framework as a hydrophobic group providing π–π stacking module. Moreover, the α-hydroxycarboxylic acid group and catechol in the structure provide double metastable binding sites with borate acid (Fig. 1A). The other *trans*-diol groups in glycosyl are relatively weak in forming boronate ester due to steric configuration.[31,40] Thus, the BA is an ideal candidate for the preparation of small-molecule hydrogel crosslinked through boronate ester.

Results and discussion

Commercially available inorganic salt $Na_2B_4O_7$ and H_3BO_3 were used as boric sources in this study. The catechol and α-hydroxycarboxylic acid group in baicalin provided stronger binding affinity with borate than other *trans*-diols. We assumed that BA will form oligomer linked by boronate ester at the beginning, which will further self-assemble through non-covalent bonds to build hydrogel. As expecting, the uniform yellow transparent hydrogel (Fig. 1A) was constructed by simple mixing BA and inorganic borate salt in deionized water with suitable pH, heating at 60 °C for 5 minutes, and then cooling down to room temperature. In aqueous media, there is an equilibrium between the acidic triangular and basic tetrahedral structure of borate ester. The equilibrium of boronate ester between dissociation and reformation relies on the pH of the environment. The boronate ester was formed usually near or above the pK_a of boric derivatives.[32] We investigated the suitable pH values for the formation of hydrogel through a vial inversion test (Fig.-S1A†). When the pH is in the range of 8.6–11.4, the mixture exhibited a semisolid state indicating the formation of the hydrogel.

The critical gelation concentration of BA and the ratio of BA/B were further confirmed at pH = 8.6. With BA/B (1 : 1), the stable gel wasn't formed until the concentration of BA increased to 200 mM (Fig. S1B†). With the boost of the concentration of BA or B, the equilibrium of reaction will move to the formation of tetrahedral boronate ester. At 50 mM, 100 mM, and 200 mM of BA, the stable gel was formed at the ratio of BA/B 1 : 4, 1 : 1.5, and 1 : 1, respectively (Fig. 1B). The scanning electron microscopy (SEM) images indicates the hydrogel consisting of a three-dimensional pore network (Fig. 1C). The pore structure had an average diameter of approximately 12.4 μm with hundreds nanometer of wall thickness (Fig. S2†). With the increase of the concentration of BA or B, the pore of three-dimensional network of hydrogel tends to become heterogeneous, and the wall of pore became thinner (Fig. S3†). The 3D pore-structure makes it the potential matrix for sustained release of drugs.

We next investigated the mechanism of gelation by characterization including NIR spectrum (Fig. 2A), and ^{1}H-NMR (Fig. 2B). In the NIR spectrum, the characteristic absorption peaks of C–H stretching vibrations at around 2925 cm^{-1}, and C=O at around 1664 cm^{-1} were transferred to the broad peaks at 2892 cm^{-1} and 1634 cm^{-1} separately, which further implied the formation of polymerization. The formation of the new broad peak at 1400 and 1154 cm^{-1} indicates the generation of boronate ester, which was consistent with the results of ^{1}H-NMR (Fig. 2B). With the addition of B, the proton peaks (H1–H9) of BA become multiple gradually. And downfield shifts of the aromatic hydrogen signals (H3 and H4) were detected, which further imply the formation of π–π stacking interactions. At BA : B = 50 : 50, the single signal of H5 became multiple broad peaks, indicating the generation of different boronate ester. And the disappearance of H7 signaling implied the hydroxycarboxylate are crucial binding sites. However, the integration of H8 and H9 didn't change. At BA : B = 50 mM : 150 mM, the proton signal became broad implying the polymerization of BA in the system. The hydrogel displayed excellent thixotropy, moldability, and self-healing properties (Fig. 2C). The hydrogel with strong mechanical strength could be ejected through the syringe without breakage and could be drawn onto glass slides without blockage in the needle. With model tools, the hydrogel was able to fabricate into various shapes such as arrow, circle, and heart (Fig. 2C). Moreover, the dynamic covalent bonds could be easily destroyed and recovered, which endowed the hydrogel with markable self-healing properties. As Fig. 2C, the crack in the gel was repaired after 2 hours after cutting. This BA/hydrogel with injectable, moldable, and self-healing properties has potential applications as the

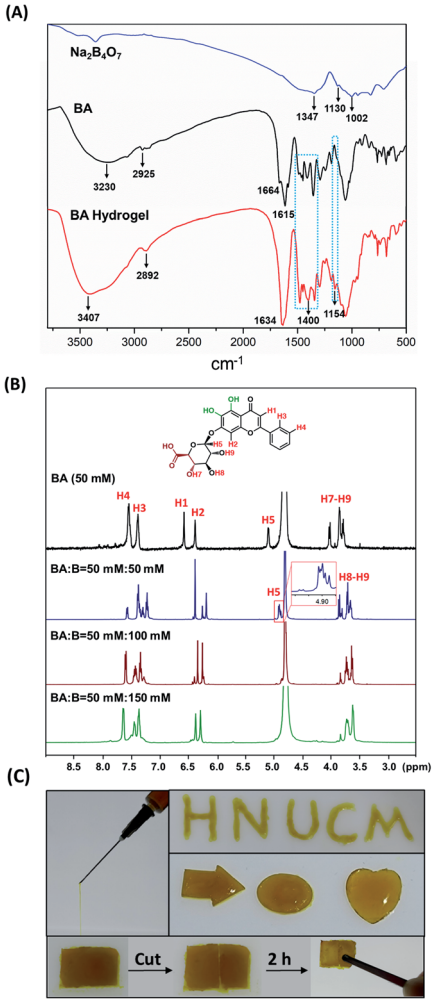

Fig. 2 Characterization of BA hydrogel. (A) NIR spectra. The BA and BA hydrogel (BA : B = 100 mM : 200 mM) were freeze-dried under pH 9.0 solution. (B) ^{1}H-NMR spectra; the BA, $Na_2B_4O_7$, were dissolved in D_2O under pH 9.0 to prepare the NMR-sample. (C) Photography of hydrogel made in different shapes.

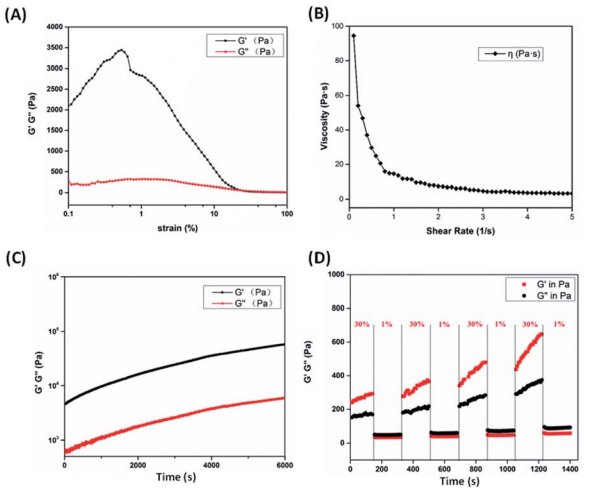

Fig. 3 Rheological tests of BA hydrogel (BA : B = 100 mM : 200 mM) at 25 °C. (A) G' and G'' of hydrogel as a function of strain at a frequency of 1 Hz; (B) viscosity with the change of shear rate. (C) G' and G'' of GL hydrogel in different time at a frequency of 1 Hz; (D) G' and G'' of BA hydrogel in alternate step strain measurements at a frequency of 1 Hz.

drug carrier for *in situ* treatments and as a type of biomaterials in 3D printing.

Rheological tests (Fig. 3) further verified the hydrogel properties. The linear viscoelastic range of the hydrogel were measured by strain sweep at a frequency of 1 Hz. Interestingly, there is no clear linear viscoelastic range for BA hydrogel. With strain lower than 0.5%, the storage modulus (G') increases slowly continuously. The hydrogel is supported by complicated intermolecular interactions between BA monomer, oligomer, free Na^+ cation, and borate ions. The increasing of G' implys the formation of intermolecular interactions and dynamic boronate esters. At low strain, the storage modulus (G') is approximately 11 times higher than loss modulus (G''), indicating intrinsic viscoelasticity of hydrogel (Fig. 3A). With the increasing of strain amplitude, the G' of hydrogel became slightly lower than G'' when strain is over 19%, implying the gel–sol transition occurred. The shear-thinning properties of hydrogel were notable according to Fig. 3B, where the viscosity dramatically decreased with the increase of shear rate. Time sweeps were performed at strain 1% and frequency 1 Hz (Fig. 3C). Unlike most shear-thinning hydrogels relying on physical crosslinking, the modulus and strength of hydrogel increased with time indicating the dynamic boronate covalent bonds in hydrogel continuously generated. In addition, the thixotropic property of hydrogel was confirmed by alternating step-strain test in Fig. 3D. The hydrogel was forced under the high strain of 30%, where the gel was destroyed and the G' was lower than the G''. Once the low strain of 1% was used, the gel was rebuilt and the G' was higher than the G''. Repeating the high-low strain cycles, the mechanical property of hydrogel was quickly repaired once withdrawing the high strain. And the modulus of hydrogel at 1% strain still kept rising (consistent with Fig. 3C), which might contribute to the dual effect of non-covalent and dynamic covalent interactions in the system. Moreover, the critical gelation temperature (CGT) of BA/$Na_2B_4O_7$ hydrogels were displayed in Fig. S4.† For BA/$Na_2B_4O_7$ hydrogels at 100 mM : 37.5 mM, 100 mM : 50 mM, and 100 mM : 100 mM, the CGT are 37, 45, and 70 °C respectively, which indicates the thermostability of BA hydrogel as injectable material. The rheological properties of hydrogel at 30 °C and 40 °C were also measured, which showed similar trend with 25 °C (Fig. S5†). With the increase of temperature, the hydrogel became sensitive to strain, indicating the thermosensitivity of BA hydrogel (Fig. S5A and B†).

The abuse of antibiotics leads to the development of drug-resistant bacteria, making it urgent to look for other sources of drugs for the treatment of bacterial infection.[41] BA has been reported to effectively destroy biofilms,[42] and inhibit the *S. aureus* quorum sensing (QS) system to prevent *S. aureus* biofilm formation.[43] QS system regulated the genes controlling virulence factors and biofilm formation of *S. aureus.* Moreover, baicalin weakens *S. aureus* pathogenicity by targeting Sortase B,

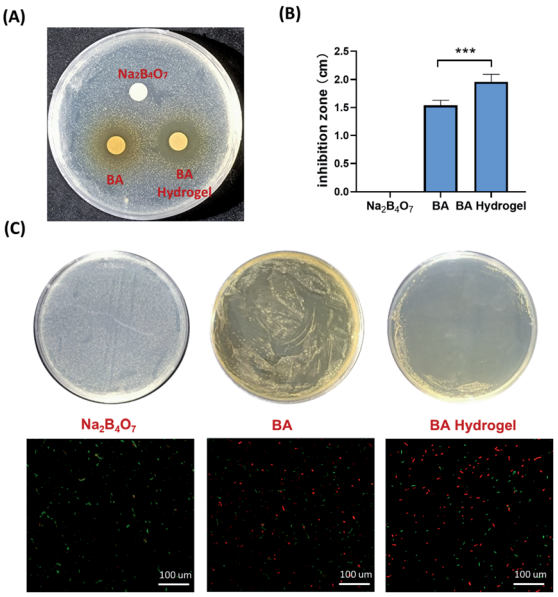

Fig. 4 The antibacterial activities of BA hydrogel. (A) The representative images of inhibition zone of $Na_2B_4O_7$, BA, and BA hydrogel after 24 h co-culturing with *S. aureus*. (B) The diameter of the inhibition zones. (C) The representative images of coating $Na_2B_4O_7$, BA, and BA hydrogel on the surface of plate with *S. aureus*, and the corresponding fluorescence images for live/dead bacterial. ***$p < 0.01$ ($n = 3$).

the crucial virulence factor of *S. aureus*. Gram-positive *S. aureus* was used to evaluate the antibacterial ability of BA hydrogel. The *S. aureus* was cultured in Luria-Bertani (LB) broth medium at 37 °C with gentle shaking. The anti-*S. aureus* property of BA hydrogel was demonstrated by an inhibition zone test. $Na_2B_4O_7$, BA suspension, and BA hydrogel (20 μL) were coated on a disc with a diameter of 6 mm, which was put on the Petri dish coating *S. aureus* overnight. As shown in Fig. 4A, the BA and BA hydrogel effectively inhibited the growth of *S. aureus*, and the control group ($Na_2B_4O_7$) show no effects on the inhibition of *S. aureus.* Comparing the inhibition zones, BA hydrogel groups were significantly larger than BA groups (Fig. 4B). The reason might be that BA hydrogel displayed higher solubility and continuous release, which support the advancement of hydrogel. Then the inhibition effects were further confirmed by coating $Na_2B_4O_7$, BA suspension, and BA hydrogel on the surface of culture plates (Fig. 4B). Compared with BA hydrogel coating on the plates easily, BA suspension was unevenly distributed on the surface of culture plates, which resulted in weak inhibition for BA suspension. The fluorescence-based live/dead assays were performed to evaluate the number of live and dead *S. aureus* in different groups (Fig. 4C). The obvious red fluorescence signals indicated that BA and BA hydrogel groups caused a dramatic increase in the number of dead *S. aureus*, which was consistent with the previous growth inhibition tests.

The behaviors of BA release from the hydrogel were studied in PBS under different pH values (Fig. 5). Regardless of high pH or low pH, the release of BA was fast at the first 12 h, and then it showed a gradual process. At pH 7.4, the release rate was around 60% after 48 h, which was attributed to the good

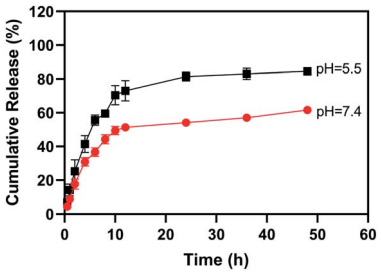

Fig. 5 Release profiles of BA from BA hydrogel (BA : B = 100 mM : 150 mM) at pH 5.5 and 7.4. Error bars represents the average ± standard deviation.

solubility of the hydrogel. At pH 5.5 the release rate was up to 85% after 48 h, which further confirmed the pH sensibility of the BA hydrogel. Moreover, to evaluate the safety of hydrogel, the human bronchial epithelial cells 16HBE were cultured with hydrogel under different BA concentrations (Fig. S6†). The cell viability showed no significant difference with or without BA hydrogel, which implied the high safety of BA hydrogel.

Experimental

Materials

Baicalin was purchased from Chengdu Herbpurify Co., Ltd (Chengdu, China, purity: 99%). Phosphate buffer solutions (PBS) were obtained from Solarbio Life Science. NaOH was purchased from Aladdin company (Shanghai, China). $Na_2B_4O_7$ was purchased from Damas-beta company (Shanghai, China). The chemicals were used as received without further purification.

Preparation and characterization of BA hydrogels

BA and $Na_2B_4O_7$ were dissolved in 1 mL double-distilled water. The pH of the mixture was adjusted to 8.6 using NaOH. A light yellow and transparent hydrogel was obtained when the mixture solution was heated at 60 °C for 5 min and slowly cooled to room temperature. FT-IR spectra were measured between 4000 and 400 cm^{-1} by a PerkinElmer Spectrum 100. ^{1}H-NMR spectra were conducted on Bruker 500 MHz NMR. Rheological measurements were performed on a HAAK Viscoteste iQ (Thermo Fisher Scientific) with a 35 mm diameter titanium parallel plate geometry. SEM images were taken on a field emission scanning electron microscope instrument (Zeiss Sigma 300).

Antibacterial assay

The antibacterial activities of BA hydrogel were evaluated by zone inhibition and spread plate methods. The *Staphylococcus aureus* (*S. aureus*) was inoculated into 5 mL Luria-Bertani (LB) broth medium and incubated at 37 °C overnight with shaking at 200 rpm. After overnight pre-culture, the bacterial suspension was diluted to 10^6 CFU mL^{-1} inoculum by PBS. The diluted bacteria were spread on the agar culture. For zone inhibition methods, the disc (diameter 6 mm) made by filter paper was

soaked by 20 μL BA (100 mM), $Na_2B_4O_7$ (50 mM), and BA hydrogel (100 mM). The dishes were put on the surface of the agar plate and co-cultured with *S. aureus* for 24 h. Then the visible inhibition zones of dishes were measured. For the spread plate method, the 100 μL BA (100 mM), $Na_2B_4O_7$ (50 mM), and BA hydrogel (100 mM) were coated on the surface of the agar plate and co-cultured with *S. aureus* for 24 h.

Live/dead fluorescent staining

The BA, $Na_2B_4O_7$, and BA hydrogel were coated on the surface of the agar plate and co-cultured with *S. aureus* for 24 h. Then *S. aureus* was collected and washed with 0.9% NaCl 3 times. The bacteria were then stained with SYTO 9 and propidium iodide (PI) from the live/dead staining kit (L7012) as the instruction. Then it was visualized with a Nikon NIS-Elements BR.

Drug release study

1 mL of BA hydrogel sample (100 mM, BA : B = 1 : 1.5) was placed into dialysis bags (MW: 3000 D) and incubated in 250 mL PBS buffer solution (pH 7.4 or pH 5.5, 0.01 M) at 37 °C. Then, 3 mL of sample was collected at each time point and replenished 3 mL of fresh PBS solution. The concentration of the sample was determined by UV/Vis absorption spectroscopy.

Cell viability

16HBE cells were cultured at 2×10^5 cells per well in 96-well plates with RPMI 1640 media plus various doses of BA hydrogels (0, 12.5, 25, 50, 100 mM) respectively for 24 h. Then the supernatant were discarded, and 10% CCK8 were added and cultured for 4 h. Absorbance was measured at 450 nm to estimate the cell viability.

Conclusions

In summary, we discovered a type of all-small-molecule dynamic covalent hydrogel consisting of natural product BA and inorganic borates such as $Na_2B_4O_7$ and H_3BO_3/NaOH. This hydrogel can be prepared by simply mixing BA and borates, avoiding tedious pre-synthesis of common polymeric materials. The BA hydrogel displayed high mechanical strength, remarkable thixotropy, moldability, and self-healing properties, which were confirmed through the rheological test. The dynamic boronate bonds endow the hydrogel with excellent degradability and multi-stimuli-responsiveness. Moreover, the mechanical strength of gel could be easily modulated by the ratio of BA to boron and the concentration of BA. The biocompatible BA hydrogel exhibited significant anti-bacterial activities, which can be used as a potential drug delivery system for *in situ* treatment. Overall, this work provided a facile strategy to prepare the small-molecule hydrogel of natural products based on dynamic covalent bonds, which broaden the family of low molecular weight gelators in fabricating gel-related biomedical materials.

Author contributions

All authors contributed to experiment conduction, data analysis, drafting or revising the article.

Conflicts of interest

There are no conflicts to declare.

Acknowledgements

This research was funded by Henan Province Scientific and Technological Project (no. 202102310472, no. 212102310344, no. 22102310638), Key scientific research project of Henan province colleges and universities (no. 22A360003), Jiansheng Fresh Medicine Innovation and Research Fund Project (jsyy-20200105-057), and National Natural Science Foundation of China (no. 82003607).

Notes and references

1 S. Naahidi, M. Jafari, M. Logan, Y. Wang, Y. Yuan, H. Bae, B. Dixon and P. Chen, *Biotechnol. Adv.*, 2017, **35**, 530–544.
2 A. Chakraborty, A. Roy, S. P. Ravi and A. Paul, *Biomater. Sci.*, 2021, **9**, 6337–6354.
3 M. Vázquez-González and I. Willner, *Angew. Chem., Int. Ed.*, 2020, **59**, 15342–15377.
4 Q. Huang, Y. Zou, M. C. Arno, S. Chen, T. Wang, J. Gao, A. P. Dove and J. Du, *Chem. Soc. Rev.*, 2017, **46**, 6255–6275.
5 S. Merino, C. Martín, K. Kostarelos, M. Prato and E. Vázquez, *ACS Nano*, 2015, **9**, 4686–4697.
6 C.-H. Lu, C.-H. Yu and Y.-C. Yeh, *Acta Biomater.*, 2021, 66–79.
7 Z. Tong, L. Jin, J. M. Oliveira, R. L. Reis, Q. Zhong, Z. Mao and C. Gao, *Bioact. Mater.*, 2021, **6**, 1375–1387.
8 B. Yang, Z. Wei, X. Chen, K. Wei and L. Bian, *J. Mater. Chem. B*, 2019, **7**, 1726–1733.
9 J. Skopinska-Wisniewska, S. De la Flor and J. Kozlowska, *Int. J. Mol. Sci.*, 2021, **22**, 7402–7425.
10 V. B. Kumar, H. Medhi, Z. Yong and P. Paik, *Nanomed.: Nanotechnol. Biol. Med.*, 2016, **12**, 579–588.
11 A. K. Yamala, V. Nadella, Y. Mastai, H. Prakash and P. Paik, *Nanoscale*, 2017, **9**, 14006–14014.
12 S. Afroz, H. Medhi, S. Maity, G. Minhas, S. Battu, J. Giddaluru, K. Kumar, P. Paik and N. Khan, *Nanoscale*, 2017, **9**, 14641–14653.
13 M. de Loos, B. L. Feringa and J. H. van Esch, *Eur. J. Org. Chem.*, 2005, **2005**, 3615–3631.
14 J. Raeburn, A. Zamith Cardoso and D. J. Adams, *Chem. Soc. Rev.*, 2013, **42**, 5143–5156.
15 B. O. Okesola and D. K. Smith, *Chem. Soc. Rev.*, 2016, **45**, 4226–4251.
16 R. Tian, J. Chen and R. Niu, *Nanoscale*, 2014, **6**, 3474–3482.
17 A. Rani, L. M. De Leon-Rodriguez, I. Kavianinia, D. J. McGillivray, D. E. Williams and M. A. Brimble, *Org. Biomol. Chem.*, 2021, **19**, 3665–3677.

18 M. Singh, S. Kundu, A. Reddy M, V. Sreekanth, R. K. Motiani, S. Sengupta, A. Srivastava and A. Bajaj, *Nanoscale*, 2014, **6**, 12849–12855.
19 H. Wang and Y. Cheng, *Mater. Chem. Front.*, 2019, **3**, 472–475.
20 W. Phurpa, *J. Biol. Act. Prod. Nat.*, 2018, **8**, 1–20.
21 Y. Cai, J. Zhang, Y. He, Z. Li, Y. Hua, Z. Wu, J. Gao, C. Ou and M. Chen, *J. Biomed. Nanotechnol.*, 2018, **14**, 257–266.
22 J. Zheng, R. Fan, H. Wu, H. Yao, Y. Yan, J. Liu, L. Ran, Z. Sun, L. Yi, L. Dang, P. Gan, P. Zheng, T. Yang, Y. Zhang, T. Tang and Y. Wang, *Nat. Commun.*, 2019, **10**, 1604.
23 J. Wang, W. Qiao, H. Zhao and X. Yang, *Biochem. Pharmacol.*, 2020, **182**, 114232.
24 T. Li, P. Wang, W. Guo, X. Huang, X. Tian, G. Wu, B. Xu, F. Li, C. Yan, X. J. Liang and H. Lei, *ACS Nano*, 2019, **13**, 6770–6781.
25 A. Saha, J. Adamcik, S. Bolisetty, S. Handschin and R. Mezzenga, *Angew. Chem., Int. Ed. Engl.*, 2015, **54**, 5408–5412.
26 X. Zhao, H. Zhang, Y. Gao, Y. Lin and J. Hu, *ACS Appl. Bio Mater.*, 2020, **3**, 648–653.
27 J. Cheng, S. Fu, Z. Qin, Y. Han and X. Yang, *J. Mater. Chem. B*, 2021, **9**, 2674–2687.
28 K. Zhi, J. Wang, H. Zhao and X. Yang, *Acta Pharm. Sin. B*, 2020, **10**, 913–927.
29 N. Iwasawa and K. Ono, *Chem. Rec.*, 2022, **22**(1), e202100214–e202100232.
30 W. Chen, X. Zhen, W. Wu and X. Jiang, *Sci. China: Chem.*, 2020, **63**, 648–664.
31 D. A. Köse, B. Zümreoglu-Karan, T. Hökelek and E. Şahin, *Inorg. Chim. Acta*, 2010, **363**, 4031–4037.
32 J. Yan, G. Springsteen, S. Deeter and B. Wang, *Tetrahedron*, 2004, **60**, 11205–11209.
33 G. Springsteen and B. Wang, *Tetrahedron*, 2002, **58**, 5291.
34 E. Aeridou, D. Díaz Díaz, C. Alemán and M. M. Pérez-Madrigal, *Biomacromolecules*, 2020, **21**, 3984–3996.
35 A. P. Bapat, B. S. Sumerlin and A. Sutti, *Mater. Horiz.*, 2020, **7**, 694–714.
36 J. H. Ryu, G. J. Lee, Y. V. Shih, T. I. Kim and S. Varghese, *Curr. Med. Chem.*, 2019, **26**, 6797–6816.
37 X. Cheng, M. Li, H. Wang and Y. Cheng, *Chin. Chem. Lett.*, 2020, **31**, 301–306.
38 S. Fu, W. Zhao, C. Xiong, L. Guo, J. Guo, Y. Qiu, C.-A. A. Hu, C. Ye, Y. Liu, Z. Wu and Y. Hou, *Innate Immun.*, 2019, **25**, 420–432.
39 L.-T. Guo, S.-Q. Wang, J. Su, L.-X. Xu, Z.-Y. Ji, R.-Y. Zhang, Q.-W. Zhao, Z.-Q. Ma, X.-Y. Deng and S.-P. Ma, *J. Neuroinflammation*, 2019, **16**, 95.
40 M. Bishop, N. Shahid, J. Yang and A. R. Barron, *Dalton Trans.*, 2004, 2621–2634, DOI: 10.1039/B406952H.
41 M. A. Ozma, E. Khodadadi, F. Pakdel, F. S. Kamounah, M. Yousefi, B. Yousefi, M. Asgharzadeh, K. Ganbarov and H. S. Kafil, *J. Herb. Med.*, 2021, **27**, 100432.
42 J. Luo, B. Dong, K. Wang, S. Cai, T. Liu, X. Cheng, D. Lei, Y. Chen, Y. Li, J. Kong and Y. Chen, *PLoS One*, 2017, **12**, e0176883.
43 G. Wang, Y. Gao, H. Wang, X. Niu and J. Wang, *Front. Cell. Infect. Microbiol.*, 2018, **8**, 418.